Upward nitrate flux and downward particulate organic carbon (POC) flux along a gradient of stratification and turbulent mixing in an Arctic shelf sea (Barents Sea)

Ingrid Wiedmann (1)
Jean-Éric Tremblay (2)
Arild Sundfjord (3)
Marit Reigstad (1)

(1) UiT The Arctic University of Norway, Breivika, Tromsø, Norway
(2) Université Laval, 3058 Québec, Canada
(3) Norwegian Polar Institute, Tromsø, Norway

Abstract

Declining sea ice cover impacts Arctic pelagic ecosystems by strengthening the stratification due to sea ice melt and exposing previously ice-covered regions to wind mixing. Here, we used the Barents Sea (BS), an Arctic shelf sea, as a model area to examine effects of wind mixing and stratification on Arctic ecosystems upward nitrate flux and the downward particulate organic carbon (POC) flux. In the northern, Arctic influenced BS, we found open drift ice and a moderate halocline stratification. This apparently hindered wind-induced deep-mixing, because the upward nitrate flux was negligible (flux into mixing layer, 13 m: 0.004 mmol nitrate m^{-2} d^{-1}) and the downward POC flux was moderate (40-200 m: 150-250 mg POC m^{-2} d^{-1}) during the ice edge diatom bloom. The Atlantic influenced, weakly stratified, ice-free southern BS was more prone to wind mixing, and we observed a high upward nitrate flux (into the mixing layer, 25 m: 5.395 mmol nitrate m^{-2} d^{-1}) and a high downward POC flux (40-120 m: 260-600 mg POC m^{-2} d^{-1}) in a post bloom situation. We suggest that the downward POC flux in a future Arctic may decline if the nitrate replenishment weakens due to halocline strengthening. However, the downward POC flux may also increase when strong winds, weak stratification and a shallow nitracline allow a pulsed nitrate replenishment in the surface layers and stimulate primary production during a summer post bloom. Enhanced downward POC flux may then either result from active down-mixing or re-packaging of biomass into fast-sinking fecal pellets by mesozooplankon.

(250 words)

1 Introduction

Arctic seas are affected by the declining sea ice cover [*Arrigo and van Dijken,* in press; *IPCC,* 2013]. Sea ice melt freshens surface waters, strengthens column stratification [*Rainville et al.,* 2011], and exposes previously ice-covered areas to wind mixing, causing shelf break upwelling and deep wind-induced mixing [*Tremblay et al.*, 2011; *Martin et al.,* 2014; *Falk-Petersen et al.,* 2015]. These changes impact Arctic pelagic ecosystems, because the intensity of the nutrient replenishment in the euphotic zone and the sedimentation of organic biomass is affected, but regulating mechanisms are still debated [*Carmack and Wassmann*, 2006; *Tremblay and Gagnon*, 2009; *Tremblay et al.*, 2011; *Wassmann and Reigstad*, 2011; *Falk-Petersen et al.*, 2015].

The Barents Sea, an Arctic shelf sea, is here used as model area to investigate the upward nitrate flux and the downward flux of particulate organic carbon (POC) in a field study under contrasting situations of hydrography and turbulent mixing (Figure 1). Arctic derived water masses [temperature $T < 0$ °C, salinity $S = 34.4\text{-}34.8$, *Loeng*, 1991] influence the northern Barents Sea, and contributes to the seasonal sea ice cover, which reaches its annual maximum extension in March/April [*Kvingedal*, 2005].When the sea ice retracts northwards during late spring and summer, sea ice melt water freshens surface waters. This strengthens the halocline and, in combination with the open drift ice, hampers wind-induced deep-mixing [*Rainville et al.*, 2011]. Surface nitrate concentrations are usually high subsequent to ice break-up, and give rise to an ice-edge related diatom bloom [*Hegseth and Sundfjord*, 2008]. This phytoplankton taxon potentially cause a major downward POC flux, such as described in the conceptual model of the northwards propagating ice edge bloom in the Barents Sea [*Sakshaug et al.,* 1991; *Sakshaug et al.*, 2009] due to the high sinking velocity of senescent stages, resting stages or aggregates [*Eppley et al.*, 1967; *Bienfang*, 1981; *Iversen and Ploug*, 2013].

Atlantic derived waters [$T > 3$ °C, $S > 35.0$, *Loeng*, 1991] influence the southern Barents Sea, where a weak stratification has been observed during the late spring and early summer [*Andreassen and Wassmann,* 1998; *Reigstad et al.*, 2002]. Accordingly, this region is more prone to wind mixing compared to the marginal ice zone. As phytoplankton growth is not light limited by sea ice in the southern Barents Sea. The onset of the bloom occurs earlier [*Leu et al.*, 2011], and, while a peak bloom still occurs at the ice edge, a post bloom stage with low nitrate concentrations may already be found in the southern Barents Sea in late June

[*Wassmann et al.*, 1999]. The low nitrate concentrations favor small cells (< 10 µm) with a high surface to volume ratio. These cells have low sinking velocities, and probably contribute little to the downward POC flux [*Mann and Lazier*, 2006]. Further, also the estimated ingestion of mesozooplankton is higher during the post bloom situation compared to the early bloom [*Wexels Riser et al.*, 2008], which enhances the POC attenuation in the water column and reduces the downward POC.

A lower downward POC flux may accordingly be presumed for the weakly stratified southern Barents Sea during a post bloom situation. However, model results for the southern Barents Sea suggested that strong winds (> 12 m s^{-1}), associated with low pressure belts, could induce deep-mixing entrain nutrients every ten days and stimulate primary production [*Sakshaug and Slagstad*, 1992]. These results were in line with measurements of wind driven turbulent mixing in the same area in summer [*Sundfjord et al.*, 2007], and potential effects on the whole pelagic ecosystem may be assumed: *Svensen et al.* [2002] observed in mesocosm studies that pulsed nitrate injections into the euphotic zone resulted in an enhanced downward POC flux, and this matches observations from the weakly stratified Barents Sea [*Olli et al.*, 2002; *Reigstad et al.*, 2008].

During the present field study, we used the Barents Sea as a model area and focused on the upward nitrate flux and downward POC flux under contrasting conditions of stratification, turbulent mixing and phytoplankton bloom along a north-south gradient from the marginal ice zone in the north to the ice-free region in the south. In this way, we aimed to (1) examine the intensity of the upward nitrate flux, (2) investigate if the upward nitrate flux considerably contributes to the nitrate stock in the upper water column, and (3) describe possible mechanisms regulating the downward POC flux under these contrasting conditions of stratification and vertical mixing.

2 Materials and Methods

Field work was carried out with the ice-enforced R/V "Helmer Hanssen" (22 – 27 June 2011) as part of the CONFLUX project. Based on a high-resolution northward CTD-F transect along the 30°E longitude (S. Basedow, pers. com.), three stations were chosen in the central Barents Sea for more detailed process studies. The north-south transect provided a gradient in

hydrography and bloom stage from the marginal ice zone in Arctic influenced waters (M1), through the Polar Front (M2) into deep-mixed, Atlantic influenced waters (M4).

2.1 Hydrography, sea ice and light conditions

Hydrography data (temperature, salinity, conductivity) and fluorescence were obtained at each station from surface to bottom (CTD-F, SeaBird 911*plus*). Data were processed with the SeaBird standard software package (bin average 0.5 m). Following *Brainerd and Gregg* [1995], we use here the term 'mixed layer' for a weakly stratified surface layer, which was not necessarily actively mixed during the time of data collection. In contrast, 'mixing layer' denotes the surface depth interval, which was actively mixed with a diffusivity > 10^{-4} m^2 s^{-1} during data collection [*Wiedmann et al.*, 2014]. Due to our focus on upward and downward transport of nitrate and organic matter, we use the term 'mixing layer' instead of the recently suggested term 'turbulent layer' [*Franks*, 2014]. The sea ice conditions were visually estimated, based on the scale of the Norwegian Meteorological Institute (11 categories from ice-free to fast ice). Underwater irradiance was measured with a GMBDH TRIOS light scanner (190-575 nm, 2.15 nm wavelength resolution) at each process station between subsurface and 20 m during local noon. The base of the euphotic zone (1 % sub-surface irradiance) was estimated for the wavelength of chlorophyll *a* (Chl *a*) [430 nm, *South and Whittick*, 1987] using the equation

$$I_D = I_0 * \exp(-k * z) \quad (1)$$

where I_D was the irradiance at depth z, I_0 the sub-surface irradiance, and k the diffuse attenuation coefficient. A minor error must be assumed, since the attenuation coefficient did not take into account the shading effects by phytoplankton at the Chl *a* maximum (located below 20 m).

2.2 Turbulence, nitrate concentrations and nitrate flux

A loosely tethered microstructure drop sonde (MSS-90L) with a pair of PNS06 shear probes [*Prandke and Stips*, 1998] was used to collect sets of 2-3 profiles roughly every four hours during station work. Only the profiles taken closest in time to the CTD and the nitrate profiles are included here. The sets of shear profiles were processed as described in *Fer* [2006], with data from above 8 m depth being discarded to avoid influence from the ship's keel. We

calculated the diffusivity K (m^2 s^{-1}) as described in [*Wiedmann et al.*, 2014]. The data were averaged over four meter moving intervals before they were used to calculate the nitrate flux.

Continuous depth profiles of nitrate were measured with a Satlantic ISUS V3 ultra-violet spectrophotometer. The accuracy of individual measurements can be up to +/- 2 mmol m^{-3} [*Johnson and Coletti*, 2002] but when several data points are averaged in vertical bins, as done here, we expect accuracy around 0.5 mmol m^{-3} [*Randelhoff et al.*, 2015]. The instrument was integrated with the ship-borne CTD system in order to get simultaneous depth data from the CTD's pressure sensor. Individual nitrate sensor spectra were processed using software provided by the manufacturer. The vertical profiles were objectively adjusted to match near-surface (10 m) nitrate concentration achieved from chemical sea water analysis [procedure following *Martin et al.*, 2010b] and smoothed using a 10 m moving average before gradients were obtained for nitrate flux calculations.

Computation of nitrate flux F_N was based on the gradient of nitrate (N) concentration with depth z and the diffusivity (K):

$$F_N = K * (dN / dz) \quad (2)$$

2.3 Nitrate uptake rates

Nitrate uptake rates are strongly dependent in the available PAR. To assess this relationship, water from the surface and the subsurface Chl *a* maximum (SCM) was collected at station M1 and M4, split in ten 500 mL tissue culture flasks each and spiked with a trace amount of ^{15}N-potassium nitrate (0.1 mM). Each set of ten flasks was placed in a separate ten-position, linear light-gradient incubator designed to minimize spectral shift [*Marcel et al.*, 1994]. Both incubators were illuminated by a single full-spectrum 400 W Optimarc metal-halide lamp mimicing solar irradiance. Optically-neutral filters (Lee Filters) were placed in front of the incubator with the surface samples to yield measured irradiances ranging from 5 to 630 µmol quanta m^{-2} s^{-1}. For the incubator with SCM samples, one layer of a blue filter (118 Light Blue Lee Filters Ltd.) was combined with optically-neutral filters (Lee Filters) to provide irradiances ranging from 3 to 365 µmol quanta m^{-2} s^{-1}. Temperature was maintained at in-situ levels with a chilling circulator. In order to minimize isotopic dilution and photo-acclimation to experimental conditions, the incubations were kept as short as possible (5-6 h) to ensure detection. Incubations were terminated by filtration onto 24 mm pre-combusted Whatman

GF/F filters. All filters were desiccated at 60 °C and stored dry for analysis ashore. An elemental analyzer (ECS 4010, Costech Analytical Technologies Inc.) coupled to a mass spectrometer (Delta V Advantage, Thermo-Finnigan) was used to determine isotopic enrichment and particulate organic nitrogen (PON) using a modified Dumas method [for details see *Blais et al.*, 2012].

Specific nitrate uptake (N) was calculated using Equation 3 of *Collos* [1987] and Uptake-irradiance parameters (and standard errors on these parameters) were calculated on specific uptake data using the double exponential model of *Platt et al.* [1980]:

$$N = N_d + N_s [1\text{-}\exp(\text{-}\alpha E / N_s)] [\exp(\text{-}\beta E / N_s)] \quad (3)$$

and

$$N_m = N_s [\alpha / (\alpha+\beta)] [\beta / (\alpha+\beta)]^{\beta/\alpha} \quad (4)$$

where N_d is the dark uptake (h^{-1}), N_s is the theoretical maximum uptake in the absence of photoinhibition (h^{-1}), N_m is the maximum observed uptake (h^{-1}), E is the incubation irradiance (PAR, µmol quanta m^{-2} s^{-1}), and α and β [h^{-1} (µmol quanta m^{-2} s^{-1})$^{-1}$] are the photosynthetic efficiency at low irradiance (initial slope of the relationship) and the photoinhibition parameter, respectively. In order to use the parameters directly in the model determining the nitrate uptake rates (calculations not shown), values were multiplied by the mean concentration of PON for the ten subsamples and divided by the concentration of Chl *a* at the depth of collection.

The continuous record of PAR on deck was combined with the vertical attenuation coefficient of underwater irradiances (k), measured at local noon, to estimate instantaneous PAR at each 1-m depth bin throughout the day. Chl *a* concentration for each depth bin was estimated by using post-calibrated in vivo fluorescence data from the CTD. For each depth bin and time of day, absolute nitrate uptake rates (µmol N L^{-1} h^{-1}) were estimated from equation (3) by substituting instantaneous PAR for E and multiplying by Chl *a*. Parameters established with the surface sample were assigned to all depths in the upper mixed layer, whereas parameters established for the SCM were used at the SCM and below it. Between the base of the mixed layer and the SCM, parameters were interpolated according to the vertical gradient of nitrate concentration for N_d and N_m, and according to depth for α and β. This procedure is justified by

the fact the nitrate concentration and depth were robust predictors of N_m and α, respectively, for the set of eight curves obtained for stations M1, M2, M3 (located between M2 and M4, not shown on Figure 1) and M4 at the surface and the SCM.

Nitrate uptake simulations in the model were run using a five days averaged record during occupation at M1 and M4 to prevent giving too much importance to short-term conditions at the time of sampling. Since running the simulation with the darkest and clearest days resulted in a variation of the depth-integrated uptake by a small variation around the mean (8-10 %), we chose to neglect this here.

2.4 Suspended and sedimented biomass (Chl *a*, POC, PON, C/N ratio)

Suspended biomass was collected with Niskin bottles attached to the CTD rosette at 12 sampling depths between subsurface and 200 m (Table 1) to construct depth profiles of Chl *a*, POC, PON and the atomic C/N ratio. A C/N ratio of 6.6 represents the Redfield ratio [*Redfield*, 1934; 1958], indicating fresh phytoplankton material. Higher ratios reflect more degraded material, or material from terrestrial origin [*Bianchi*, 2006]. Collected water was gently transferred from Niskin bottles and stored cool and dark until filtration within few hours. Triplicates (50-200 mL) of each depth were vacuum-filtered onto Whatman GF/F filters (pore size 0.7 µm) and Whatman Nucleopore membrane filters (pore size 10 µm) to achieve a size-fractionation of the Chl *a* containing material (total and > 10 µm). Chl *a* was extracted in 5 mL methanol (12 h, room temperature, darkness) and the Chl *a* concentration was measured using a Turner Design 10-AU fluorometer (calibrated with Chl *a*, Sigma C6144), applying the acidification method [*Holm-Hansen and Riemann*, 1978]. For POC and PON, triplicates (200 mL) of each sampling depth were filtered on pre-combusted Whatman GF/F filters. Larger organisms such as copepods or chaetognats were removed before the filters were frozen (-20 °C) until analyses (< 6 months). Analyses were carried out using a Leeman Lab CHN Elemental Analyzer [for details see *Reigstad et al.*, 2008].

A neutrally buoyant free-floating sediment trap array was deployed for ~20-24 h at M1, M2 and M4 (Table 1). Semi-Lagrangian drifting was ensured, by anchoring the trap array on an ice-floe at M1 and M2. At M4 the trap array was freely drifting in open waters, but with the buoyancy located below the surface to minimize the wind drift. Paired trap cylinders (KC Denmark, outer diameter 72 mm, length 450 m) were mounted at the sampling depths (40, 50, 60, 90, 120 and 200 m). The content of the cylinders was transferred into carboys after recovery and stored cool and in darkness until filtered in triplicates (200 mL, swimmers were

removed as far as possible) and analyzed as described previously for suspended POC and PON.

2.5 Calculations

Upward nitrate flux and the nitrate uptake of autotrophs affect the nitrate stock in the surface layer. We run a simple model (Table 2) to investigate the interaction of both factors in detail in different biological important depth intervals, such as the layer with a nitrate stock < 1 mmol nitrate m^{-3} (nitrate limitation), the depth interval between the surface and the SCM, the euphotic zone (irradiance > 1 % of the sub-surface irradiance), the mixed layer and the mixing layer (see definition section 2.1). The contribution of the upward nitrate flux to the stock (% input from below, Table 2) was calculated as the ratio of the upward nitrate flux to the integrated nitrate concentration in each layer. The time to nitrate exhaustion without upward nitrate flux equals the ratio of the integrated nitrate stock to the integrated nitrate uptake above the base of the respective layer. For the time to nitrate exhaustion with upward nitrate flux, we put up a model calculation, which starts with the integrated nitrate stock in a certain depth layer (e.g. mixing layer) and assumed for each consecutive day a constant nitrate uptake and a certain upward nitrate flux (see Table 2 for the chosen conditions).

3 Results

3.1 Hydrography, euphotic zone and wind

Station M1 in the northern Barents Sea was covered with very open drift ice (Table 1, Figure 1). A staircase-like halocline (7-23 m) structured the water column in a well-mixed meltwater affected layer in the upper 7 m (temperature T = -1.2 °C, salinity S = 32.9) and a water layer of Arctic origin gradually mixed with some Atlantic water at depth (25-200 m: T < 0 °C, S = 34.0-34.7, Figure 2a). The base of the euphotic zone with 1 % irradiance (430 nm) was located at 65 m (Figure 2d). M2 was located in very open drift ice in the Polar Front (Table 1). In this area, colder and fresher Arctic derived water masses tend to cover warmer and more saline Atlantic derived water [*Loeng*, 1991]. This was also observed during our study (Figure 2b): A well-mixed meltwater layer (0-15 m: T < 0.0 °C, S = 32.6) was separated by a strong halocline (15-20 m) from the lower part of the water column, which was, increasingly with depth, influenced by Atlantic water (200 m: T = 0.9 °C, S = 35.0). The euphotic zone reached down to 54 m (Figure 2e). The southernmost station M4 in the ice-free, Atlantic

influenced, southern part of the Barents Sea (Figure 1), was weakly stratified by a mainly temperature driven pycnocline at 35-40 m (Figure 2c). Above 35 m, we found water masses characterized by T > 5.0 °C and a salinity of 35.09, while a gradually decreasing temperature (40 m: T = 3.5 °C, 200 m: T = 2.3 °C) and a fairly constant salinity (S = 35.10 -35.13) was observed below. The base of the euphotic zone was situated to 45 m (Figure 2f). We observed strong winds during station work at M1 (9.5-13.3 m s^{-1}) and previous to station work at M4 (6.7-13.5 m s^{-1}).

3.2 Nitrate concentration, vertical diffusivity, and nitrate flux

At M1, nitrate was nearly depleted in the upper 20 m (Figure 3a). Surface-enhanced mixing (diffusivity > 10^{-4} m^2 d^{-1}) protruded to 13 m, but due to the negligible nitrate concentrations in this depth interval, the high diffusivity resulted in a low nitrate flux (Figure 3g). The nitracline, here defined as the depth interval of the sharp increase in nitrate concentration, was located between 20 and ~40 m (Figure 3a). Diffusivity was low in the 15-25 m interval, because of the staircase like halocline in this depth interval. Between ca. 25 and nearly 40 m, stratification was weaker than in the 15-25 m depth interval and the nitrate concentration increased with depth, resulting in a nitrate flux of ~0.4 mmol m^{-2} d^{-1}. Below 40 m, nitrate fluxes were estimated to be < 0.1 mmol m^{-2} d^{-1} (Figure 3g). The upward nitrate flux into the biological significant depth intervals was calculated and found to be negligible when compared to the integrated nitrate stock (< 0.4 % d^{-1}, Table 2).

At M4, nitrate concentrations increased from the (near-)surface (1 m: < 0.1 mmol nitrate m^{-3}) down to ~73 m (7.54 mmol nitrate m^{-3}, Figure 3b) and an enhanced diffusivity (> 10^{-4} m^2 d^{-1}) was found in the uppermost 25 m (Figure 3h). The upward nitrate flux into the euphotic zone (0-45 m, Table 2), the mixed layer (0-38 m) as well as layer above the SCM (0-45 m) was small compared to the nitrate stock in these layers (< 1 % d^{-1}, Table 2). However, the upward nitrate flux added 12 % d^{-1} and 38 % d^{-1} to the nitrate stock in the zone of < 1 mmol nitrate m^{-3} (0-27 m) and the mixing layer (0-25 m, Table 2), respectively.
The minor decline in concentration below the maximum values (~70 m, Figure 3a, b) likely reflects differences in advection history at the different subsurface depths or may be a small artifact related to the accuracy of the nitrate sensor.

3.3 Suspended biological parameters (size fractionated Chl *a*, POC, C/N ratio)

At station M1, the most pronounced sub-surface Chl *a* maximum (40 m: 4.4 mg Chl *a* m^{-3}) was observed, dominated by large cells (> 10 µm, Figure 2d). The suspended POC also showed a distinct sub-surface peak at 40 m, but the Chl *a* and POC depth distribution was strongly linked (R^2 = 0.91). A C/N ratio of 7.5-9.5 (1-50 m) indicated little to moderately degraded biomass in this depth interval (Figure 2g).

A subsurface Chl *a* peak was also found at M2 (44 m: 1.5 mg Chl *a* m^{-3}), but it was weaker when compared to M1 and dominated by small cells (50-80 %, Figure 2e). The POC maximum at 40 m (Figure 2h) was only weakly correlated to Chl *a* (R^2 = 0.56). A C/N ratio of 8.1-9.2 was observed in the uppermost 50 m (Figure 2h).

Also at M4 we found a sub-surface Chl *a* maximum (45 m: 1.6 mg m^{-3}, dominated by small cells, Figure 2f). The suspended POC was here evenly distributed in the uppermost 40 m (330-360 mg POC m^{-3}, Figure 2i), before abruptly declining to "background" concentrations of ~120-130 mg m^{-3} (60-200 m). This pattern was also observed at M1 and M2. Chl *a* and POC concentration were weakly correlated at M4 (R^2 = 0.60), and the vertical distribution of C/N ratio was comparable to M1 and M2 (Figure 2i).

Based on the integrated nitrate concentrations, which were highest at M1 and lowest at M4 (Figure 3a, b), as well as the phyto-/ zooplankton composition and abundance [*Wiedmann et al.*, 2014], the three stations M1, M2 and M4 were classified as a late peak bloom stage, late bloom stage and post bloom stage, respectively.

3.4 Nitrate uptake rates and time to nitrate exhaustion

The nitrate uptake rate at M1 peaked at 32 m (2.5 mmol nitrate m^{-3} $d^{-1,}$ Figure 3c), and the estimated time to nitrate exhaustion reached its minimum of 5.3 days in the depth layer 0-35 m (Figure 3e). At M4 the maximum nitrate uptake rate was found at 37 m (0.4 mmol nitrate m^{-3} d^{-1}, Figure 3d). Our nitrate model indicates that the time to nitrate exhaustion was shortest in the layers 0-38 m and 0-42 m (~9.4 d, Figure 3f).

According to our model, nitrate concentrations in the mixing layer of M1 (13 m) were exhausted after 15 days if the upward nitrate flux was set to zero (Table 2). When including the upward nitrate flux of 0.004 nitrate m^{-2} d^{-1}, the time to exhaustion was prolonged to 16 days (Table 2).

The model suggested for M4, that nitrate concentrations would become exhausted in the mixing layer (0-25 m) after 10 days if the upward nitrate flux was set to zero. The observed

upward nitrate flux rate at M4 was however high at 25 m (5.39 mmol nitrate m^{-2} d^{-1}). We presume that this was linked to the strong winds for 1-3 days during the passage of low pressure fronts, but that a relaxation would take place after this period (assumed flux: 0.30 mmol nitrate m^{-2} d^{-1}, equaling the average flux between 50 and 70 m, which was a depth interval not influenced by surface mixing processes). Depending on the number of days with strong mixing (1-3 days), our model suggested that nitrate would be exhausted in the mixing layer after 16, 21 or 25 days, respectively (Table 2).

3.4 Characterization of the vertical flux (POC, C/N ratio)

The intensity of the vertical POC flux and the C/N ratio of the sedimenting material varied between the stations.

The POC flux (at 120 m) was highest at M4 (261 mg POC m^{-2}) compared to the other stations (156-187 mg POC m^{-2} d^{-1}). The attenuation of the flux, calculated from the depth of the highest flux (M1: 90 m, M2 and M4: 40 m) to 120 m, was weakest at M1 (~20 %) and higher at the other stations (56 and 65 % at M2 and M4, respectively).

Along the stratification gradient from the north to the south, we found a declining trend of the C/N ratio (Figure 4), implying that sinking material was more degraded at M1 and M2 than at M4.

4 Discussion

In our field study, we used the Barents Sea as a model area to investigate the upward nitrate flux, the impacts on the nitrate stock in the upper water column and the downward POC flux under contrasting hydrographical and phytoplankton bloom situations along the north-south gradient. We found a negligible upward nitrate flux and a moderate downward POC flux in Arctic influenced waters at the ice edge in the north, and high upward nitrate and downward POC fluxes in the Atlantic influenced waters and discuss in the following if water column stratification and vertical mixing were drivers of these fluxes.

4.1 Impact of water column stratification and vertical turbulent mixing on the upward nitrate flux

The vertical nitrate flux (Equation 1) in the water column is linked to the diffusivity in the water column [*Osborn*, 1980; *Moum*, 1996] and the vertical gradient of the nitrate

concentration. Diffusivity is low in strongly stratified waters and thus restrains the vertical nitrate flux. In contrast, tide and wind mixed waters have a high diffusivity, which drives the nitrate flux together. The nitrate concentration determines the nitrate flux intensity by the steepness of its slope with depth, and governs the flux direction, because the nitrate flux follows Fick's Law of diffusion from high to low concentrations. An upward nitrate flux is commonly observed in marine ecosystems, because primary production in the euphotic zone mainly depletes nitrate close to the surface while high concentrations are found at depth [Figure 3g, h; *Mann and Lazier*, 2006].

At our northernmost station, the combination of a moderately strong halocline, following the ice break-up and melting, and the partial sea ice cover hampered deep turbulent mixing [*Le Fouest et al.*, 2011; *Rainville et al.*, 2011], resulting in a negligible upward nitrate flux (< 0.04 mmol nitrate m^{-2} d^{-1}) into biologically interesting layers (Table 2). The low fluxes were comparable to previous studies from a stratified, partly ice-covered location in the northern Barents Sea [upward nitrate flux into the upper mixed layer during a summer ice edge bloom: 0.14 mmol nitrate m^{-2} d^{-1}, *Sundfjord et al*., 2007], the ice-free northeast Atlantic subpolar gyre [upward nitrate flux in the upper mixed layer during summer: 0.02-0.60 mmol nitrate m^{-2} d^{-1}, *Painter et al*., 2014] and the Porcupine Abyssal Plain, NE Atlantic [upward nitrate flux into the euphotic zone during a weakly stratified summer situation: 0.09 mmol N m^{-2} d^{-1}, *Martin et al.*, 2010a].

The ice-free, weakly stratified waters at M4 were more prone to surface forced wind mixing, resulting in a considerable upward nitrate flux (> 5 mmol m^{-2} d^{-1}, Table 2) into the base of the mixing layer (Figure 3 g, h). This nitrate flux was up to two orders of magnitude higher than observed flux at the respective depth at M1 (Table 2), but comparable intensities of upward nitrate fluxes were observed in other deep-mixed locations, such as the southern Barents Sea during late July [nitrate flux into the base of the upper mixed layer: 2.4 mmol nitrate m^{-2} d^{-1}, *Sundfjord et al.*, 2007] and the tidally mixed Celtic Sea during summer [nitrate flux into the base of the SCM: 1.3-9 mmol nitrate m^{-2} d^{-1}, *Sharples et al*., 2007].

The upward nitrate flux at the Polar Front (data not shown) had an intermediate strength when compared to M1 and M2 and our data accordingly suggest a gradual change in terms of upward nitrate flux from marginal ice zone to ice-free waters in the Barents Sea.

The restricted nitrate replenishment in the euphotic zone at the ice edge region matches previous suggestions for the subpolar North Atlantic. In this area, convective winter mixing

was pointed out to be a period of major upward nutrient flux [*Louanchi and Najjar*, 2001], because thermal stratification tends to hamper deep vertical wind mixing during the summer [e.g., NE Atlantic, *Martin et al.*, 2010a; *Painter et al.*, 2014]. Nitrate replenishment during early summer, such as observed here, was also reported from the southeast Bering Shelf [*Sambrotto et al.*, 1986]. We suggest it may be a phenomenon restricted to high latitude seas [*Townsend et al.*, 1992; *Eilertsen*, 1993], where phytoplankton blooms take place in unstratified waters and warming of the surface and thermocline stratification occurs during summer.

4.2 Impact of water column stratification and turbulent mixing on the nitrate stock of the upper water column

The nitrate concentrations during our field study were low at the surface, but enhanced at depth (> 6 mmol m^{-3} at 100 m, Figure 3a, b), which corresponded to previously observed spring bloom scenarios in the region [*Reigstad et al.*, 2002; *Hodal and Kristiansen*, 2008]. When modelling the effect of the upward nitrate flux and the nitrate uptake rates on the nitrate stock in different layers (Table 2), our data show that time until nitrate exhaustion was shorter at M4 than at M1 if the upward nitrate flux is not taken into account. We anticipated that this was due to the combination of a higher nitrate uptake rate (< 24 m) and a lower integrated nitrate concentration at M4 than at M1 (Table 2).

In the model runs with upward nitrate flux, the time to nitrate exhaustion in the mixing layer was only prolonged by one day at M1, because of the generally low upward nitrate flux and the minor contribution of the upward nitrate flux to the stock (0.0-0.4 % d^{-1}, Table 2) at this station. A correspondingly low daily injection into the upper mixed layer (< 0.5 % of the nitrate stock d^{-1}) was found in the subpolar Atlantic Ocean gyre [*Painter et al.*, 2014], but we wondered if the low upward nitrate flux (0.035 mmol nitrate m^{-2} d^{-1}) resembled the reality at M1. The marginal ice zone moved northward subsequent to our station work and the location was ice-free by 27 June 2011 (ice map from the Norwegian Meteorological Institute, http://157.249.32.242/archive/). Ice melt probably strengthened the halocline stratification [*Sundfjord et al.*, 2008], and created a strong stratified system such as the one found at M2. We chose in the set-up of our model therefore to use an upward nitrate flux of 0.035 mmol nitrate m^{-2} d^{-1} (such as observed at M1) for 5 days, followed by an upward flux equaling the one into the base of the mixing zone at M2 (~0.35 mmol nitrate m^{-2} d^{-1}). This enhanced upward nitrate flux prolonged the time to nitrate exhaustion in the mixing layer to 45 days at

M1. Nevertheless, a constant decline of the nitrate concentrations is suggested by the model run, because the nitrate uptake rates always exceeded the upward nitrate flux. We assume that this situation would have triggered a gradual transition from system based on nitrate production to a regenerative, post bloom system, such as described for the spring-summer transition e.g. in the Arctic Kongsfjorden, Svalbard [*Iversen and Seuthe*, 2011].
Alternatively, it would be possible that strong wind mixing after disappearance of all sea ice caused a break down the stratification and induce mixing. Model results of this scenario by *Sundfjord et al.* [2008] suggest a mixing in the uppermost 10-20 m, but not deeper. This pinpoints that no considerable deepening of the mixing layer occurred, and we consider our model assumptions as reliable.

Deep-mixing and the observed high upward nitrate flux in the ice-free waters at M4 were assumed to be rather linked to a passing low pressure front than to be a constant trait of the system in the southern Barents Sea. In the model, we used therefore a 1-3 days of deep-mixing followed by relaxation (Table 2). The calculations still indicate that one day of high upward nitrate flux could prolong the time to nitrate exhaustion in the mixing layer by six days (Table 2). A two day deep-mixing doubled the time to nitrate exhaustion and a three-day deep-mixing replenished the nitrate concentration so much, that the initial nitrate concentration would be reached after seven consecutive days of low upward flux and constant nitrate uptake. This matches well with the rhythmic pattern of wind peaks occurring every 10 days [*Sakshaug and Slagstad*, 1992].
Accordingly, we suggest, that a weak stratified water column and strong wind mixing below the nitracline could replenished nitrate concentrations in the mixing layer of the ice-free Barents Sea, because the intensity of the upward nitrate flux exceeded the nitrate uptake rate more than 3-fold. Enhanced nitrate concentrations in the surface could however not be observed in this field study. Our short stay at the station (ca. 24 h) could be considered as one reason, but we rather suggest that no build-up in nitrate concentration took place, but that nitrate was immediately been taken up by the abundant cells of the phytoplankton taxon *Phaeocystis pouchetii* (ca. 1.8 x 10^6 cells L^{-1}) [*Wiedmann et al.*, 2014].

4.3 Impact of water column stratification and turbulent mixing on the downward POC flux

The intensity of the downward POC flux reflects the hydrographical situation and the planktonic ecological interactions in the water column above. High biomass sedimentation

events tend to occur, when a weak temporal coupling of primary production and maximum grazer activity allows for sinking of biomass, such as suggested for the northward propagating ice edge in the Barents Sea [*Sakshaug et al.*, 1991; *Sakshaug et al.*, 2009; *Wassmann and Reigstad*, 2011].

POC flux rates of 150-1000 mg POC m^{-2} d^{-1} ($\geq$ 40 m) have been observed in this region during the present study and match previous measurements in this region during the same season [*Andreassen and Wassmann*, 1998; *Coppola et al.*, 2002; *Olli et al.*, 2002; *Reigstad et al.*, 2008]. We propose that a combination of factors promoted the downward POC flux at the ice edge during the present study. The high Chl *a*: POC ratio at M1 suggests that suspended autotrophs were the prevailing form of particulate organic carbon in the water column, and aggregates of large diatoms (> 10 µm) have been identified as the prevailing vehicle of vertically exported biomass to ≤60 m [*Wiedmann et al.*, 2014]. These aggregates can sink with few meters to few hundred meters per day, depending on species and physiological stage [*Bienfang et al.*, 1982; *Iversen and Ploug*, 2013]. Also, mesozooplankton abundances were low at M1 when compared to M2 and M4 [*Wiedmann et al.*, 2014, *Svensen et al*., in prep.], and caused a low attenuation of the sinking biomass at this northernmost station.

The downward POC flux at the weakly stratified station M4 exceeded the one observed at M1. Similarly high downward fluxes have previously been observed the deep-mixed, Atlantic influenced part of the southern Barents Sea [*Reigstad et al*., 2008: early bloom 400-750 mg POC m^{-2} d^{-1} at 30-200 m], though a post bloom situation is often associated with a minor POC sedimentation [*Wassmann and Reigstad*, 2011]. We suggest that the wind-induced deep-mixing stimulated the downward POC flux in different ways. The abundant prymnesiophyte *Phaeocystis pouchetii* [*Wiedmann et al.*, 2014] has a low sinking velocity, but its cells may contribute to the downward POC flux when down-mixing occurs such as at M4 [*Reigstad and Wassmann*, 2007]. This line of argumentation is bolstered by the low C/N ratio of the sedimenting material (C/N = 6.4-7.7, Figure 4), suggesting a fast downwards transport of recently produced biomass.

Along our north-south transect, the mesozooplankton abundance increased toward south [*Svensen et al*., in prep.]. We assume that these grazers executed an intense top-down control especially at M4 and caused the strong POC attenuation. Pulsed nitrate supply stimulates primary production, such as described from the southeastern Bering Sea [*Sambrotto et al.*, 1986]. In situations of high zooplankton abundance, the increased primary production may cause enhanced feeding rates of copepods and the production of larger fecal pellets [*Turner*

503 *and Ferrante,* 1979, and references therein; *Wexels Riser et al.*, 2007]. Following Stokes'
504 Law, a higher sinking velocity must be assumed for these larger pellets, and they obviously
505 enhanced the downward POC flux, because they were frequently observed in the sediment
506 traps at M4 [*Wiedmann et al.*, 2014].
507 In summary, we suggest that deep-mixing enhanced the downward POC flux in the weakly
508 stratified water column at M4 in two ways: pulsed upward nitrate flux events stimulated
509 primary production and the produced biomass was both actively down-mixed and repackaged
510 into large mesozooplankton fecal pellets with high sinking velocity.
511
512

513 # 5. Conclusion

514 This field study was conducted along a north-south located transect in the central Barents Sea,
515 an Arctic shelf sea. We used it as a model area to study upward nitrate and downward POC
516 flux along a gradient of turbulent surface mixing, water column stratification and bloom stage.
517 At the northernmost, moderately stratified, station at the ice edge, a negligible upward nitrate
518 flux and a moderate downward POC flux was found during a late peak bloom dominated by
519 planktonic diatoms. The situation largely resembled the conceptual model of a northward
520 propagating ice edge phytoplankton bloom (Figure 5) [*Sakshaug et al.*, 1991; *Sakshaug et al.*,
521 2009].
522 In the weakly stratified, Atlantic influenced waters of our southernmost station we found a
523 contrasting situation. Wind-induced deep-mixing reached here down to 35-40 m, and
524 enhanced the upward nitrate flux considerably. This apparently stimulated the primary
525 production and the produced biomass was (1) actively down-mixed and (2) utilized by the
526 abundant zooplankton community and repackaged into fast-sinking fecal pellets, which
527 enhanced the downward POC flux. Accordingly, we recommend extending the conceptual
528 model of a northward propagating ice edge phytoplankton bloom by a deep-mixed, post
529 bloom situation with high downward POC flux towards the south (Figure 5).
530 The present study shows that there are two possible mechanisms of a considerable downward
531 POC flux in Arctic pelagic ecosystems; one coupled to the ice edge phytoplankton bloom and
532 another one, which is linked to an ice-free, weakly stratified water column. Re-occurring
533 strong winds may here induce deep-mixing below the nitracline during the productive
534 summer season, stimulate primary production and enhance the biomass sedimentation. In a
535 perspective of climate warming, these results indicate that the downward POC flux not

necessarily ceases if sea ice declines and ice edge phytoplankton blooms are restricted to smaller areas, because an enhanced downward POC flux may also take place in weakly stratified ice-free Arctic regions, where strong winds induce an upward nitrate flux. However, a warming Arctic climate will most likely also strengthens thermal warming of the surface layers during summer [*Wassmann and Reigstad*, 2011] and impact stratification in the water column. This factor has not been regarded in the present study, but needs further attention in the future.

Acknowledgements

We thank the captain and the crew of the R/V "Helmer Hanssen" for practical support during the field work. Sigrid Øygaarden, Christian Wexels Riser and Camilla Svensen helped with field and laboratory work and this was highly appreciated. The present work is a part of the Conflux project, funded by Tromsø Forskningsstiftelse, but also financially supported by the CarbonBridge project (Norwegian Research Council, no. 226415). A. Sundfjords's participation was partially funded by the Center of Ice, Climate and Ecosystem (ICE) at the Norwegian Polar Institute.

Literature

Andreassen, I. J., and P. Wassmann (1998), Vertical flux of phytoplankton and particulate biogenic matter in the marginal ice zone of the Barents Sea in May 1993, *Mar. Ecol. Prog. Ser.*, *170*, 1-14.

Arrigo, K. R., and G. L. van Dijken (in press), Continued increases in Arctic Ocean primary production, *Prog. Oceanogr.*, doi:10.1016/j.pocean.2015.05.002.

Bianchi, T. S. (2006), *Biochemistry of Estuaries*, Oxford University Press, Cary, USA.

Bienfang, P. K. (1981), Sinking rates of heterogeneous, temperate phytoplankton populations, *J. Plankton Res.*, *3*(2), 235-253, doi:10.1093/plankt/3.2.235.

Bienfang, P. K., P. J. Harrison, and L. M. Quarmby (1982), Sinking rate response to depletion of nitrate, phosphate and silicate in four marine diatoms, *Mar. Biol.*, *67*(3), 295-302.

Blais, M., J.-É. Tremblay, A. D. Jungblut, J. Gagnon, J. Martin, M. Thaler, and C. Lovejoy (2012), Nitrogen fixation and identification of potential diazotrophs in the Canadian Arctic, *Global Biogeochem. Cy.*, *26*(3), GB3022, doi:10.1029/2011GB004096.

Brainerd, K. E., and M. C. Gregg (1995), Surface mixed and mixing layer depths, *Deep-Sea Res. I*, *42*(9), 1521-1543, doi:10.1016/0967-0637(95)00068-H.

Carmack, E., and P. Wassmann (2006), Food webs and physical–biological coupling on pan-Arctic shelves: Unifying concepts and comprehensive perspectives, *Prog. Oceanogr.*, *71*(2–4), 446-477, doi:10.1016/j.pocean.2006.10.004.

Collos, Y. (1987), Calculations of ^{15}N uptake rates by phytoplankton assimilating one or several nitrogen sources, *Int. J. Radiat. Appl. Instrum. Part A.*, *38*(4), 275-282, doi:10.1016/0883-2889(87)90038-4.

Coppola, L., M. Roy-Barman, P. Wassmann, S. Mulsow, and C. Jeandel (2002), Calibration of sediment traps and particulate organic carbon export using ^{234}Th in the Barents Sea, *Mar. Chem.*, *80*(1), 11-26, doi:10.1016/S0304-4203(02)00071-3.

Eilertsen, H. C. (1993), Spring blooms and stratification, *Nature*, *363*(6424), 24-24, doi:10.1038/363024a0.

Eppley, R. W., R. W. Holmes, and J. D. H. Strickland (1967), Sinking rates of marine phytoplankton measured with a fluorometer, *J. Exp. Mar. Biol. Ecol.*, *1*(2), 191-208, doi:10.1016/0022-0981(67)90014-7.

Falk-Petersen, S., V. Pavlov, J. Berge, F. Cottier, K. Kovacs, and C. Lydersen (2015), At the rainbow's end: high productivity fueled by winter upwelling along an Arctic shelf, *Polar Biol.*, *38*(1), 5-11, doi:10.1007/s00300-014-1482-1.

Fer, I. (2006), Scaling turbulent dissipation in an Arctic fjord, *Deep-Sea Res. I*, *53*(1–2), 77-95, doi:10.1016/j.dsr2.2006.01.003.

Franks, P. J. S. (2014), Has Sverdrup's critical depth hypothesis been tested? Mixed layers vs. turbulent layers, *ICES J. Mar. Sci.*, 1-11, doi:10.1093/icesjms/fsu175.

Hegseth, E. N., and A. Sundfjord (2008), Intrusion and blooming of Atlantic phytoplankton species in the high Arctic, *J. Mar. Syst.*, *74*(1–2), 108-119, doi:10.1016/j.jmarsys.2007.11.011.

Hodal, H., and S. Kristiansen (2008), The importance of small-celled phytoplankton in spring blooms at the marginal ice zone in the northern Barents Sea, *Deep-Sea Res. II*, *55*(20–21), 2176-2185, doi:10.1016/j.dsr2.2008.05.012.

Holm-Hansen, O., and B. Riemann (1978), Chlorophyll *a* Determination: Improvements in Methodology, *Oikos*, *30*(3), 438-447, doi:10.2307/3543338.

IPCC (Ed.) (2013), *Climate Change 2013: The Physical Science Basis. Contribution of Working Group I to the Fifth Assessment Report of the Intergovernmental Panel on Climate Change*, 1535 pp., Cambridge University Press, Cambridge, United Kingdom and New York, NY, USA, doi:10.1017/CBO9781107415324.

Iversen, K. R., and L. Seuthe (2011), Seasonal microbial processes in a high-latitude fjord (Kongsfjorden, Svalbard): I. Heterotrophic bacteria, picoplankton and nanoflagellates, *Polar Biol.*, *34*(5), 731-749, doi:10.1007/s00300-010-0929-2.

Iversen, M. H., and H. Ploug (2013), Temperature effects on carbon-specific respiration rate and sinking velocity of diatom aggregates - potential implications for deep ocean export processes, *Biogeosciences*, *10*(6), 4073-4085, doi:10.5194/bg-10-4073-2013.

Johnson, K. S., and L. J. Coletti (2002), In situ ultraviolet spectrophotometry for high resolution and long-term monitoring of nitrate, bromide and bisulfide in the ocean, *Deep-Sea Res. I*, *49*(7), 1291-1305, doi:10.1016/S0967-0637(02)00020-1.

Kvingedal, B. (2005), Sea-Ice Extent and Variability in the Nordic Seas, 1967—2002, in *The Nordic Seas: An Integrated Perspective*, edited by H. Drange, T. Dokken, T. Furevik, R. Gerdes and W. Berger, pp. 39-49, American Geophysical Union, Washington, D. C.. doi:10.1029/158GM04.

Le Fouest, V., C. Postlethwaite, M. A. Morales Maqueda, S. Bélanger, and M. Babin (2011), On the role of tides and strong wind events in promoting summer primary production in the Barents Sea, *Cont. Shelf Res.*, *31*(17), 1869-1879, doi:10.1016/j.csr.2011.08.013.

Leu, E., J. E. Søreide, D. O. Hessen, S. Falk-Petersen, and J. Berge (2011), Consequences of changing sea-ice cover for primary and secondary producers in the European Arctic shelf seas: Timing, quantity, and quality, *Progr. Oceanogr.*, *90*(1–4), 18-32, doi:10.1016/j.pocean.2011.02.004.

Loeng, H. (1991), Features of the physical oceanographic conditions of the Barents Sea, *Polar Res.*, *10*(1), 5-18, doi:10.1111/j.1751-8369.1991.tb00630.x.

Louanchi, F., and R. G. Najjar (2001), Annual cycles of nutrients and oxygen in the upper layers of the North Atlantic Ocean, *Deep-Sea Res. II*, *48*(10), 2155-2171, doi:10.1016/S0967-0645(00)00185-5.

Mann, K., and J. Lazier (2006), *Dynamics of Marine Ecosystems: Biological-Physical Interactions in the Oceans, Third Edition*, Blackwell Publishing.

Marcel, B., A. Morel, and R. Gagnon (1994), An incubator designed for extensive and sensitive measurements of phytoplankton photosynthetic parameters, *Limnol. Oceanogr.*, *39*(3), 694-702, doi:10.4319/lo.1994.39.3.0694.

Martin, A. P., M. I. Lucas, S. C. Painter, R. Pidcock, H. Prandke, H. Prandke, and M. C. Stinchcombe (2010a), The supply of nutrients due to vertical turbulent mixing: A study at the Porcupine Abyssal Plain study site in the northeast Atlantic, *Deep-Sea Res. II*, *57*(15), 1293-1302, doi:10.1016/j.dsr2.2010.01.006.

Martin, J., J.-É. Tremblay, J. Gagnon, G. Tremblay, A. Lapoussiére, C. Jose, M. Poulin, M. Gosselin, Y. Gratton, and C. Michel (2010b), Prevalence, structure and properties of subsurface chlorophyll maxima in Canadian Arctic waters, *Mar. Ecol. Prog. Ser.*, *412*, 69-84, doi:10.3354/meps08666.

Martin, T., M. Steele, and J. Zhang (2014), Seasonality and long-term trend of Arctic Ocean surface stress in a model, *J. Geophys. Res.-Oceans*, *119*(3), 1723-1738, doi:10.1002/2013JC009425.

Moum, J. N. (1996), Efficiency of mixing in the main thermocline, *J. Geophys. Res.*, *101*(C5), 12057-12069, doi:10.1029/96JC00508.

Olli, K., C. W. Rieser, P. Wassmann, T. Ratkova, E. Arashkevich, and A. Pasternak (2002), Seasonal variation in vertical flux of biogenic matter in the marginal ice zone and the central Barents Sea, *J. Mar. Syst.*, *38*, 189-204, doi:10.1016/S0924-7963(02)00177-X

Osborn, T. R. (1980), Estimates of the Local Rate of Vertical Diffusion from Dissipation Measurements, *J. Phys. Oceanogr.*, *10*(1), 83-89, doi:10.1175/1520-0485(1980)010<0083:EOTLRO>2.0.CO;2.

683 Painter, S. C., S. A. Henson, A. Forryan, S. Steigenberger, J. Klar, M. C. Stinchcombe, N. Rogan, A.
684 R. Baker, E. P. Achterberg, and C. M. Moore (2014), An assessment of the vertical diffusive flux of
685 iron and other nutrients to the surface waters of the subpolar North Atlantic Ocean, *Biogeosciences*,
686 *11*(8), 2113-2130, doi:10.5194/bg-11-2113-2014.
687
688 Platt, T., C. L. Gallegos, and W. G. Harrison (1980), Photoinhibition of photosynthesis in natural
689 assemblages of marine phytoplankton, *J. Mar. Res.*, *38*, 687-701.
690
691 Prandke, H., and A. Stips (1998), Test measurements with an operational microstructure-turbulence
692 profiler: Detection limit of dissipation rates, *Aquat. Sci.*, *60*(3), 191-209, doi:10.1007/s000270050036.
693
694 Rainville, L., C. M. Lee, and R. A. Woodgate (2011), Impact of wind-driven mixing in the Arctic
695 Ocean, *Oceanography*, *24*(3), 136, doi:10.5670/oceanog.2011.65.
696
697 Randelhoff, A., A. Sundfjord, and M. Reigstad (2015), Seasonal variability and fluxes of nitrate in the
698 surface waters over the Arctic shelf slope, *Geophys. Res. Lett.*, *42*(9), 3442-3449,
699 doi:10.1002/2015GL063655.
700
701 Redfield, A. C. (1934), On the proportion of organic derivates in sea water and their relation to the
702 composition of plankton, in *James Johnstone Memorial Volume*, edited, pp. 177-192, Liverpool
703 University Press, Liverpool.
704
705 Redfield, A. C. (1958), The biological control of chemical factors in the environment, *Am. Sci.*, *46*(3),
706 205-221.
707
708 Reigstad, M., and P. Wassmann (2007), Does *Phaeocystis* spp. contribute significantly to vertical
709 export of organic carbon?, *Biogeochemistry*, *83*(1-3), 217-234, doi:10.1007/s10533-007-9093-3.
710
711 Reigstad, M., C. W. Riser, P. Wassmann, and T. Ratkova (2008), Vertical export of particulate organic
712 carbon: Attenuation, composition and loss rates in the northern Barents Sea, *Deep-Sea Res. II*, *55*,
713 2308-2319, doi:10.1016/j.dsr2.2008.05.007.
714
715 Reigstad, M., P. Wassmann, C. Wexels Riser, S. Øygarden, and F. Rey (2002), Variations in
716 hydrography, nutrients and chlorophyll a in the marginal ice-zone and the central Barents Sea, *J. Mar.*
717 *Syst.*, *38*(1–2), 9-29, doi:10.1016/S0924-7963(02)00167-7.
718
719 Sakshaug, E., and D. Slagstad (1992), Sea ice and wind: Effects on primary productivity in the Barents
720 Sea, *Atmos. Ocean*, *30*(4), 579-591.
721
722 Sakshaug, E., S. Kristiansen, and E. Syvertsen (1991), Planktonalger, in *Økosystem Barentshav*, edited
723 by E. Sakshaug, A. Bjørge, F. Gulliksen, H. Loeng and F. Melhum, Universitetsforlaget, Oslo.
724
725 Sakshaug, E., G. Johnsen, S. Kristiansen, C. von Quillfeldt, F. Rey, D. Slagstad, and F. Thingstad
726 (2009), Phytoplankton and primary production, in *Ecosystem Barents Sea*, edited by E. Sakshaug, G.
727 Johnsen and K. Kovacs, pp. 167-208, Tapir Academic Press, Trondheim, Norway.
728
729 Sambrotto, R. N., H. J. Niebauer, J. J. Goering, and R. L. Iverson (1986), Relationships among vertical
730 mixing, nitrate uptake, and phytoplankton growth during the spring bloom in the southeast Bering Sea
731 middle shelf, *Cont. Shelf Res.*, *5*(1–2), 161-198, doi:10.1016/0278-4343(86)90014-2.
732
733 Sharples, J., J. F. Tweddle, J. Mattias Green, M. R. Palmer, Y.-N. Kim, A. E. Hickman, P. M.
734 Holligan, C. M. Moore, T. P. Rippeth, and J. H. Simpson (2007), Spring-neap modulation of internal
735 tide mixing and vertical nitrate fluxes at a shelf edge in summer, *Limnol. Oceanogr*, *52*(5), 1735-1747.
736

South, G. R., and A. Whittick (1987), *An Introduction to Phycology*, Wiley-Blackwell.

Sundfjord, A., I. Fer, Y. Kasajima, and H. Svendsen (2007), Observations of turbulent mixing and hydrography in the marginal ice zone of the Barents Sea, *J. Geophys. Res.-Oceans*, *112*, C05008, doi:10.1029/2006JC003524.

Sundfjord, A., I. Ellingsen, D. Slagstad, and H. Svendsen (2008), Vertical mixing in the marginal ice zone of the northern Barents Sea—Results from numerical model experiments, *Deep-Sea Res. II*, *55*(20–21), 2154-2168, doi:10.1016/j.dsr2.2008.05.027.

Svensen, C., J. C. Nejstgaard, J. K. Egge, and P. Wassmann (2002), Pulsing versus constant supply of nutrients (N, P and Si): effect on phytoplankton, mesozooplankton and vertical flux of biogenic matter, *Sci. Mar.*, *66*(3), 189-203.

Townsend, D. W., M. D. Keller, M. E. Sieracki, and S. G. Ackleson (1992), Spring phytoplankton blooms in the absence of vertical water column stratification, *Nature*, *360*(6399), 59-62, doi:10.1038/360059a0.

Tremblay, J.-É., and J. Gagnon (2009), The effects of irradiance and nutrient supply on the productivity of Arctic waters: a perspective on climate change, in *Influence of Climate Change on the Changing Arctic and Sub-Arctic Conditions*, edited by J. C. J. Nihoul and A. G. Kostianoy, pp. 73-93, Springer Netherlands, doi:10.1007/978-1-4020-9460-6_7.

Tremblay, J. É., S. Bélanger, D. G. Barber, M. Asplin, J. Martin, G. Darnis, L. Fortier, Y. Gratton, H. Link, P. Archambault, A. Sallon, C. Michel, W. J. Williams, B. Philippe, and M. Gosselin (2011), Climate forcing multiplies biological productivity in the coastal Arctic Ocean, *Geophys. Res. Lett.*, *38*(18), L18604, doi:10.1029/2011GL048825.

Turner, J. T., and J. G. Ferrante (1979), Zooplankton Fecal Pellets in Aquatic Ecosystems, *Bioscience*, *29*(11), 670-677, doi:10.2307/1307591.

Wassmann, P., and M. Reigstad (2011), Future Arctic Ocean seasonal ice zones and implications for pelagic-benthic coupling, *Oceanography*, *24*(3), 220-231, doi:10.6570/oceanog.2011.74.

Wassmann, P., T. Ratkova, I. Andreassen, M. Vernet, G. Pedersen, and F. Rey (1999), Spring Bloom Development in the Marginal Ice Zone and the Central Barents Sea, *Mar. Ecol. , 20*(3-4), 321-346, doi:10.1046/j.1439-0485.1999.2034081.x.

Wexels Riser, C., P. Wassmann, M. Reigstad, and L. Seuthe (2008), Vertical flux regulation by zooplankton in the northern Barents Sea during Arctic spring, *Deep-Sea Res. II*, *55*(20–21), 2320-2329, doi:10.1016/j.dsr2.2008.05.006.

Wexels Riser, C., M. Reigstad, P. Wassmann, E. Arashkevich, and S. Falk-Petersen (2007), Export or retention? Copepod abundance, faecal pellet production and vertical flux in the marginal ice zone through snap shots from the northern Barents Sea, *Polar Biol.*, *30*(6), 719-730, doi:10.1007/s00300-006-0229-z.

Wiedmann, I., M. Reigstad, A. Sundfjord, and S. Basedow (2014), Potential drivers of sinking particle's size spectra and vertical flux of particulate organic carbon (POC): Turbulence, phytoplankton, and zooplankton, *J. Geophys. Res.-Oceans*, *119*(10), 6900-6917, doi:10.1002/2013JC009754.

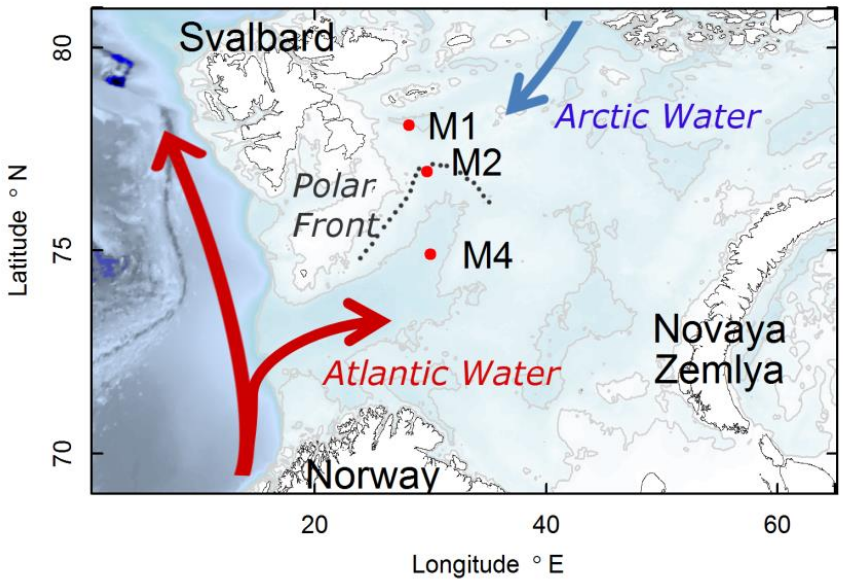

Figure 1: Map showing the Barents Sea with the three sampling stations (M1, M2, M4). Hydrography in the Barents Sea is influenced by Atlantic derived water (entering from the southwest) and Arctic derived water (entering from the northeast).

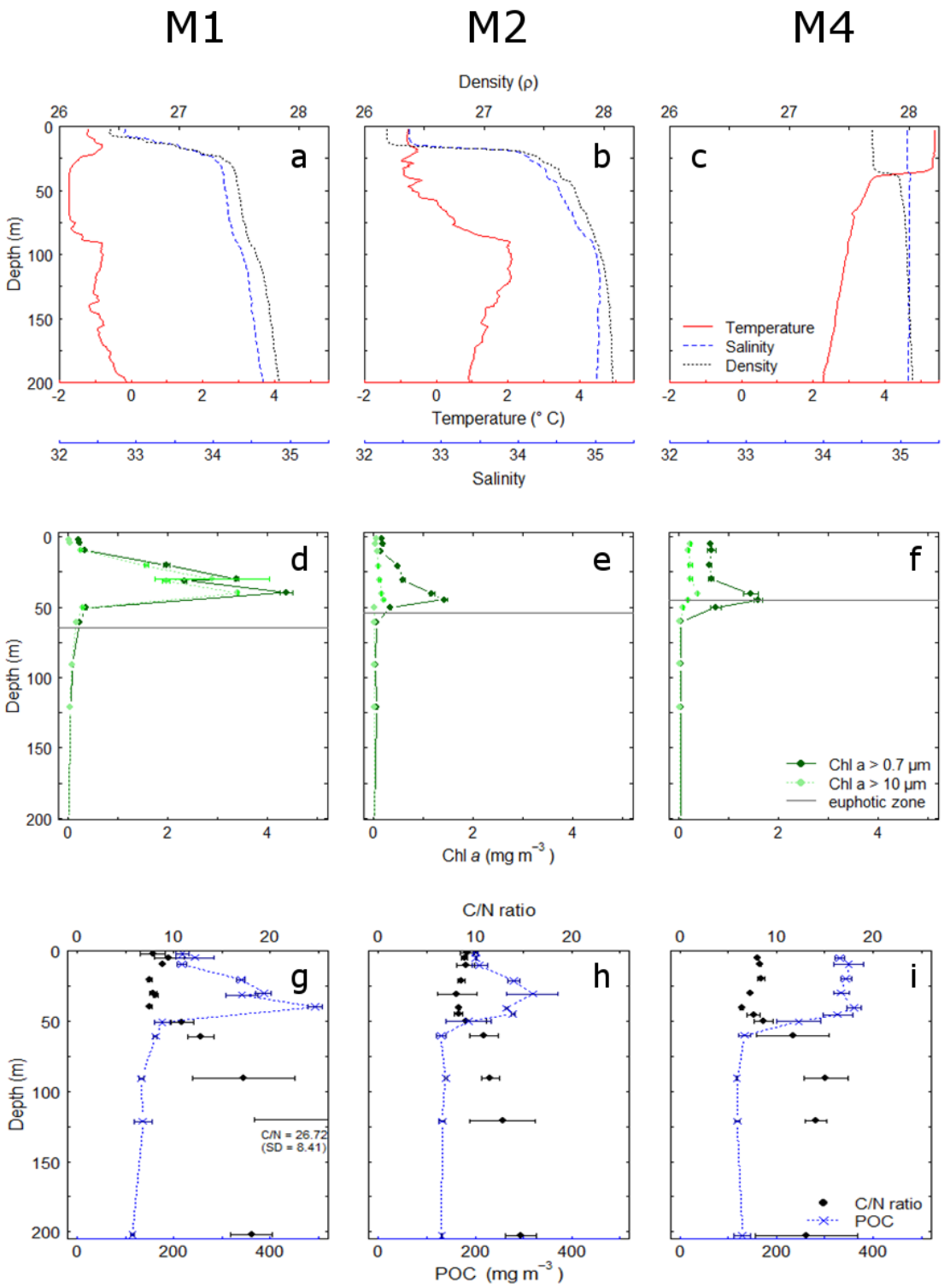

Figure 2: Hydrography with temperature (red line), salinity (blue stippled) and density black dotted) in upper panel (a, b, c), irradiance (grey line) and suspended chlorophyll *a* (Chl *a*, dark green: total Chl *a*, light green: > 10 µm) in middle panel (d, e, f) as well as suspended particulate organic carbon (POC) and atomic C/N ratio in the lower panel (g, h, i) of the upper 200 m at M1 (left column), M2 (middle column) and M4 (right column).

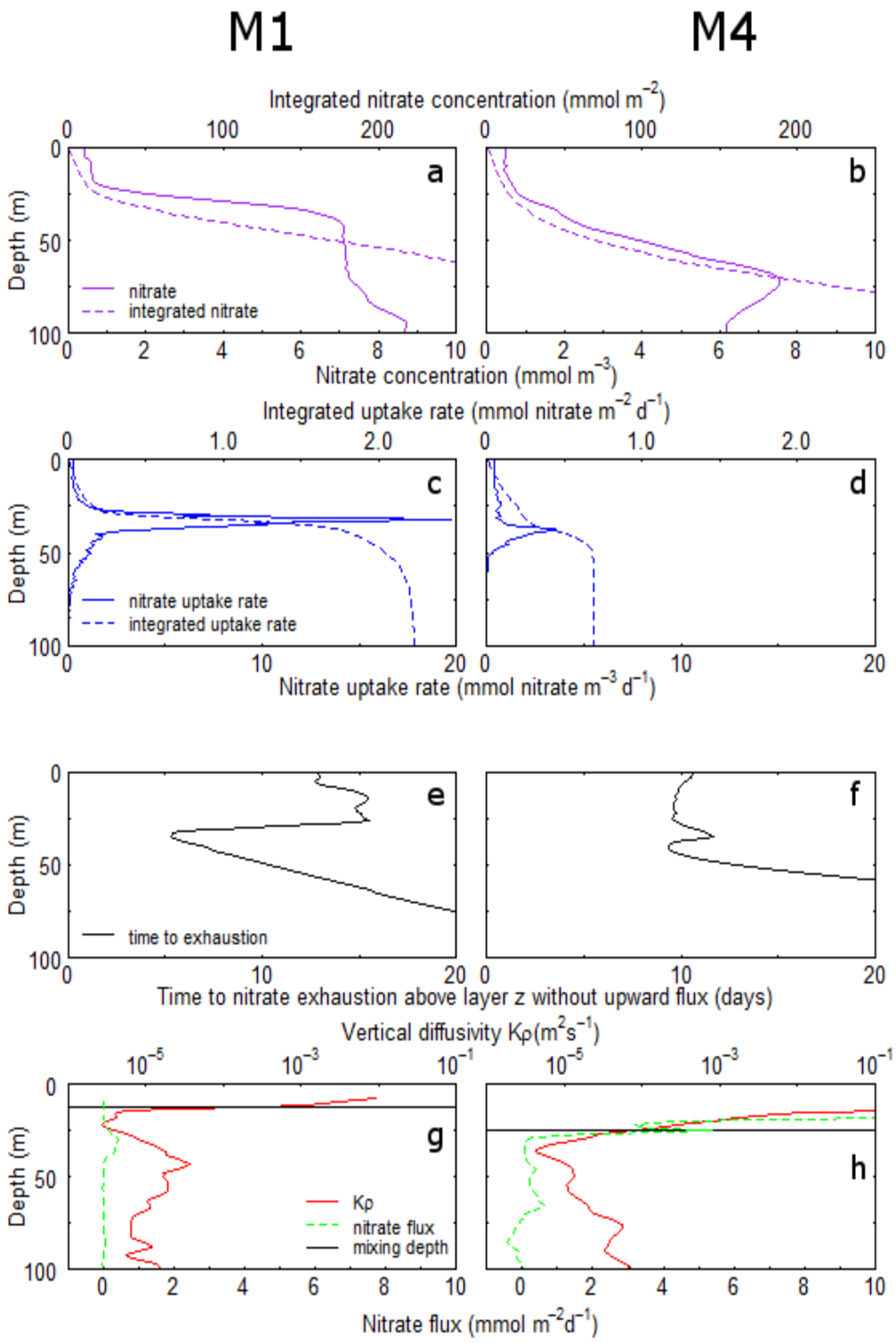

Figure 3: Nitrate concentrations (a, b; line: concentration, dotted: integrated concentration), nitrate uptake rate (c, d; line: uptake rate, dotted: integrated uptake rate), time to nitrate exhaustion (e, f) and vertical diffusivity (g, h, red line) and the upward nitrate flux (g, h, green dotted) in the upper 100 m of the water column at M1 (left column) and M4 (right column).

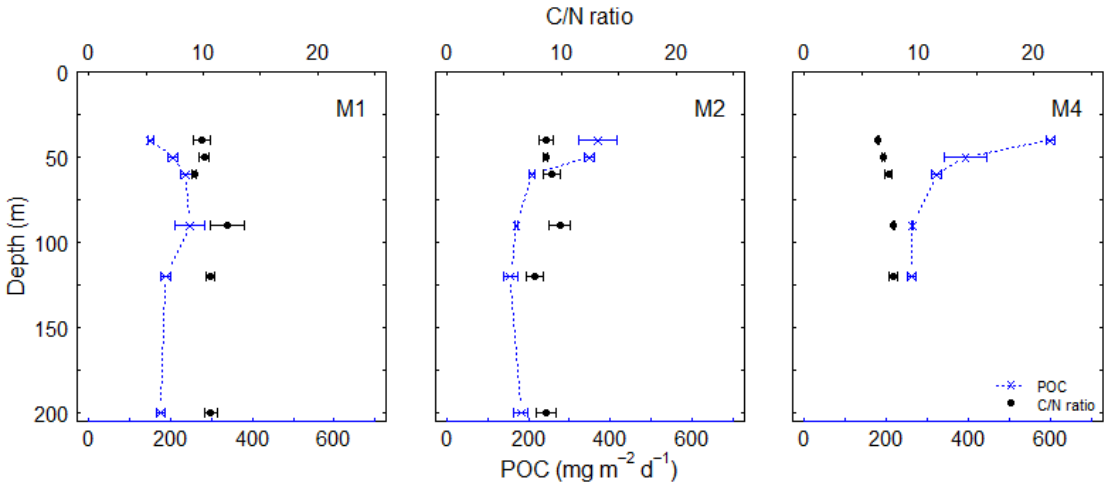

Figure 4: Vertical flux of particulate organic carbon (POC, blue crosses, bars indicating the standard deviation) and the C:N ratio of the sedimenting material (black dots, bars indicating the standard deviation) atM1 (left), M2 (middle) and M4 (right). The 200 m sample was not available for M4.

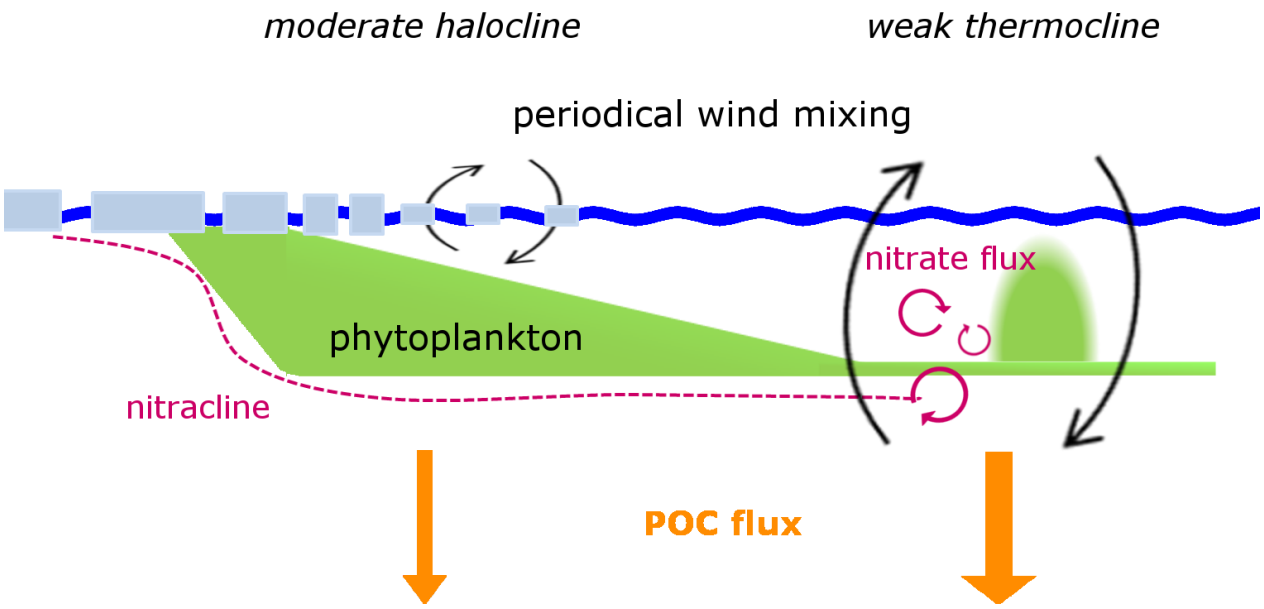

Figure 5: Conceptual model of the phytoplankton bloom in the marginal ice zone and the associated downward flux of particulate organic carbon (POC). Figure modified from a model developed by *Sakshaug et al*., [1991] and *Sakshaug et al*., [2009] for the Barents Sea. Model was extended to include upward nitrate flux and downward POC flux events associated with the periodical wind-induced deep-mixing.

Table 1: Station identity and sampling schedule.

	Position	Date	Depth (m)	Ice cover	Chl *a* max (m)	Suspended sampling (UTC)[1]	Deployment trap array (UTC)[2]	Deploy-ment time (d)
M1	78.0973°N, 28.1258°E	22 June 2011	278	Very Open Drift Ice (30%)	31	16:45	23:30	0.85
M2	76.9493°N, 29.7117°E	24 June 2011	235	Very Open Drift Ice (20%)	44	07:46	16:15	0.94
M4	74.9107°N, 30.0033°E	27 June 2011	371	Open Water	45	09:11	16:55	0.98

[1]sampled parameters: chlorophyll *a* (Chl *a*), particulate organic carbon (POC) and nitrogen (PON); 1, 5, 10, 20, 30, 40, 50, 60, 90, 120, 200 m and Chl *a* maximum

[2]sampled parameters: POC and PON: 40, 50, 60, 90, 120, 200 m

Table 2: Compilation of the integrated nitrate stock in different biological interesting layers and the upward nitrate flux into these layers. See section 2.4 for an explanation of the calculations. SCM: subsurface chlorophyll *a* maximum.

	Depth interval	Nitrate stock in the layer (mmol m^{-2})	Upward nitrate flux into the base of the layer (mmol m^{-2} d^{-1})	% input from below (d^{-1})	Time to nitrate exhaustion (no upward nitrate flux) (d)	Time to nitrate exhaustion (with upward nitrate flux) (d)
M1						
Nitrate < 1 mmol m^{-3}	0-21 m	13.1	0.046	0.4	15	
Above SCM	0-40 m	99.8	0.068	0.1	16	
Euphotic zone	0-65 m	277.9	0.008	0.0	9	
Mixed layer	0-23 m	15.7	0.063	0.4	15	
Mixing layer	0-13 m	7.3	0.004	0.0	15	16[1], 45[2]
M4						
Nitrate < 1 mmol m^{-3}	0-27 m	16.3	1.948	12.0	10	
Above SCM	0-45 m	52.1	0.340	0.7	10	
Euphotic zone	0-45 m	52.1	0.340	0.7	10	
Mixed layer	0-38 m	34.2	0.108	0.3	10	
Mixing layer	0-25 m	14.4	5.395	37.4	10	16[3], 21[4], 25[5]

(1) constant upward nitrate flux 0.004 mmol m^{-2} d^{-1}
(2) nitrate upward flux 0.004 mmol m^{-2} d^{-1} for 5 days, then constant upward nitrate flux of 0.350 mmol m^{-2} d^{-1}
(3) nitrate upward flux of 5.395 mmol m^{-2} d^{-1} for 1 day, then constant upward nitrate flux of 0.300 mmol m^{-2} d^{-1}
(4) nitrate upward flux of 5.395 mmol m^{-2} d^{-1} for 2 days, then constant upward nitrate flux of 0.300 mmol m^{-2} d^{-1}
(5) nitrate upward flux of 5.395 mmol m^{-2} d^{-1} for 3 days, then constant upward nitrate flux of 0.300 mmol m^{-2} d^{-1}